

Finite-Difference Time-Domain Simulation of Wave Transmission Through Space-Time-Varying Media

Sajjad Taravati, *Senior Member, IEEE*

Abstract—This paper presents a comprehensive study on the generalized Finite Difference Time Domain (FDTD) numerical modelling of electromagnetic wave scattering from space-time-varying media. We investigate the dynamic behavior of generalized oblique and normal incidence of both TM and TE electromagnetic fields on space-time-modulated gratings. In their most general form, these gratings have electrical permittivity, magnetic permeability, and electrical conductivity modulated across both space and time. The FDTD scheme and equations for both TM and TE wave illuminations of space-time-varying slabs are provided. Additionally, intriguing illustrative examples are presented, including the nonlinear multi-beam-multi-frequency generator and linear pure beam-splitting frequency generation for generalized oblique TM wave incidence, as well as the antenna-mixer-amplifier, nonreciprocal slab, diffraction grating, and nonreciprocal beamsplitter for TE wave incidence. Through these examples, we showcase the versatility and potential applications of space-time-varying microwave components in modern communication systems, and quantum technologies.

Index Terms—FDTD, numerical simulation, time modulation, metamaterials, Maxwell’s equations, wave scattering.

I. INTRODUCTION

SPACE-TIME-MODULATED metamaterials and metasurfaces have garnered significant attention due to their wide-ranging applications in modern wireless communication systems, quantum computing, photonics, radar technologies, and beyond [1]–[10]. These structures exhibit dynamic properties characterized by the modulation of electrical permittivity, magnetic permeability, and electrical conductivity across both space and time [11]–[19]. Understanding their behavior is crucial for designing advanced devices and systems with enhanced functionality and performance.

Analyzing wave propagation in these media and the associated physical phenomena necessitates a deep comprehension of electrodynamics and electromagnetics, including Lorentz transformations [20], electromagnetic wave propagation, and wave-vector diagrams in space-time periodic media [15], [21]–[27], as well as unique analytical implications [28], [29]. Space-time metasurfaces can be realized at microwave [30]–[33] and optical frequencies [9], [34], [35] for various functionalities, including nonreciprocal transmission [10], [31], [32], [36], target recognition [37], isolators [14], [38], temporal aiming [39], pure frequency conversion [40], [41], static-to-dynamic field conversion [42], circulators [43], [44], parametric amplification [45], [46], multiple access secure communication systems [6], [47], nonreciprocal antennas [48], [49],

coding metasurfaces [50], and multifunctional operations [8], [51].

However, current commercial electromagnetic simulation software packages lack efficient tools for effectively simulating these dynamic and sophisticated structures, hindering the rapid development and optimization of space-time-varying microwave components. To address this gap, this paper presents a generalized and well-defined Finite Difference Time Domain (FDTD) numerical simulation scheme for modeling linear and nonlinear space-time-varying media. We apply the FDTD method to simulate electromagnetic wave scattering from space-time modulated media. These media exhibit properties that vary both spatially and temporally, introducing additional complexity into the simulation. The time-varying permittivity $\epsilon(z, t)$, permeability $\mu(z, t)$, and conductivity $\sigma(z, t)$ of the medium must be incorporated into the updating equations to accurately model the electromagnetic behavior. Detailed equations and methodologies for both TE and TM wave illuminations of space-time-varying slabs are provided to facilitate fast and accurate simulation of these complex structures. By offering a versatile and efficient tool through our proposed FDTD scheme, researchers and engineers gain access to a platform for investigating the dynamic behavior of space-time-varying microwave components. This advancement enables the rapid development and optimization of novel microwave devices with tailored functionalities, fostering progress in communication systems, radar technologies, and various engineering applications.

The paper is organized as follows. Section II provides an overview of different categories of space, time, and space-time metamaterials and metasurfaces, detailing their unique properties. Section III introduces the fundamentals of FDTD simulation for space-time-varying media, including the Courant stability factor, and the behavior of the refractive index and electromagnetic fields in these media. Section IV details the FDTD simulation scheme and electromagnetic fields update equations for generalized oblique TM wave incidence and transmission through space-time-varying media. Section V describes the FDTD simulation scheme and electromagnetic fields update equations for generalized oblique TE wave incidence and transmission through space-time-varying media. Section VI presents illustrative examples and functionalities. Finally, Sec. VII concludes the paper, summarizing key findings and implications.

S. Taravati is with the Faculty of Engineering and Physical Sciences, University of Southampton, Southampton SO17 1BJ, UK (e-mail: S.Taravati@soton.ac.uk).

Manuscript received ***, 2024; revised ***, 2024.

II. TIME-VARYING METAMATERIALS AND METASURFACES

Figure 1 illustrates the Minkowski space of 12 distinct categories of MMs & MSs, classified based on the dependencies of their refractive index n on space and time. This includes, spatial abrupt discontinuity $n_{r>r_0} = n_2$, temporal abrupt discontinuity $n_{t>t_0} = n_2$, spatiotemporal abrupt discontinuity $n_{\{r>r_0;t>t_0\}} = n_2$, spatial photonic crystals $n(\mathbf{r})$, temporal photonic crystals $n(t)$, spatiotemporal photonic crystals $n(\mathbf{r}, t)$, linear spatially-modulated media $n(\beta\mathbf{r})$, linear temporally-modulated media $n(\omega t)$, linear spatiotemporally-modulated media $n(\beta\mathbf{r}, \omega t)$, nonlinear spatially-modulated media $n(\mathbf{I}; \mathbf{r})$, nonlinear temporally-modulated media $n(\mathbf{I}; t)$, and nonlinear spatiotemporally-modulated media $n(\mathbf{I}; \mathbf{r}, t)$.

Minkowski space, also known as spacetime, is a cornerstone of modern physics, particularly in Einstein's special relativity. This mathematical framework unifies space and time into a single, four-dimensional fabric, where both are treated equally. Unlike our classical view of separate three-dimensional space and one-dimensional time, Minkowski space integrates them into a cohesive whole. A key concept in this framework is the idea of events, which are points in spacetime defined by specific spatial coordinates (\mathbf{r}) and time coordinates (t). These coordinates (\mathbf{r} and t) are crucial for pinpointing the location and timing of events, enabling a precise and thorough understanding of physical phenomena. In the realm of MMs & MSs, Minkowski space becomes particularly relevant when considering the behavior of electromagnetic waves. By visualizing these variations within the framework of Minkowski space, researchers can gain deeper insights into how these materials interact with electromagnetic waves, paving the way for innovative applications in fields such as wireless communications, biomedicine and quantum technologies.

Linear space-modulated MMs & MSs represented by $n(\mathbf{r})$ are materials whose refractive index varies spatially but does not depend on the intensity of the optical signal. These materials exhibit spatial modulation of the refractive index, which can be controlled to manipulate the propagation of light. Nonuniform transmission lines serve as examples of linear space-modulated media. Over the past decade, linear materials with dependence on time $n(t)$ and space-time $n(\mathbf{r}, t)$ are widely studied. Taking advantage of phase-engineered $n(t)$ MMs & MSs, several enhanced efficiency apparatuses and novel functionalities have been reported, including nonreciprocal-beam MS, ideal frequency converter MS, low-noise isolators and circulators, and enhanced resolution imaging. The $n(r, t)$ MMs & MSs break time reversal symmetry by employing unidirectional STM. The applicant's work in this area has led to innovative designs for non-reciprocal and multifunctional components, including one-way beam-splitter, antenna-mixer-amplifier, mixer-duplexer-antenna, pure frequency convertor, and magnet-less isolators. This breakthrough enables the integration of signal processing and antenna functionality within a singular MM framework, heralding a new class of multifunctional systems. Nonlinear materials $n(\mathbf{I})$ like SCs show properties that change with current intensity. Nonlinear space-modulated MMs & MSs

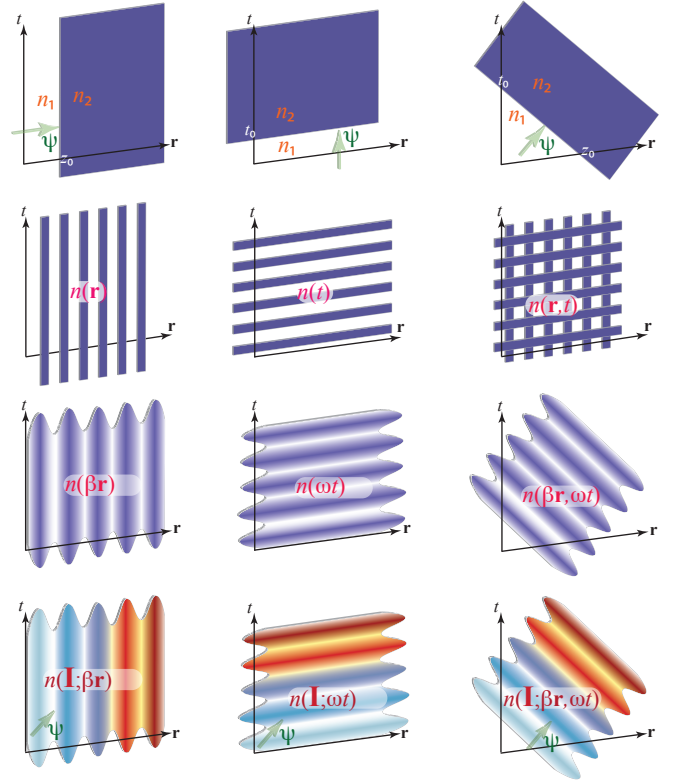


Fig. 1. Representation of space-time inhomogeneous media in four-dimensional Minkowski space: 1st column: Spatially inhomogeneous (variations in space). 2nd column: Temporally inhomogeneous (variations in time). 3rd column: Spatiotemporally inhomogeneous (variations in both space and time).

represented by $n(\mathbf{I}; \mathbf{r})$ are materials whose refractive index varies both spatially and nonlinearly with the intensity of the optical signal. These materials combine spatial modulation with nonlinear optical effects, enabling complex control over light propagation and interactions. Nonlinear Bragg gratings and photonic crystals with engineered nonlinearities are a prominent example of nonlinear space-modulated MMs & MSs. These gratings consist of periodic variations in the refractive index along the length of an optical fiber, and the intensity-dependent refractive index allows for nonlinear phenomena such as soliton formation and optical switching.

Nonlinear space-time-modulated media are represented by $n(\mathbf{I}, t) = n_0(t) + n_2(t)\mathbf{I}(t)$ and $n(\mathbf{I}, \mathbf{r}, t) = n_0(\mathbf{r}, t) + n_2(\mathbf{r}, t)\mathbf{I}(\mathbf{r}, t)$. Here, $n_0(\mathbf{r}, t)$ represents the spatial and temporal variation of the linear refractive index, $n_2(\mathbf{r}, t)$ represents the spatial and temporal variation of the nonlinear refractive index coefficient, and $\mathbf{I}(\mathbf{r}, t)$ represents the spatial and temporal variation of the intensity of the signal. Over the past decade, linear STM $n(\mathbf{r}, t)$ has emerged as a significant advance for enabling nonreciprocal wave transmission, offering a clear advantage over traditional methods that use bulky, expensive magnetic ferrites incompatible with integrated circuit technology and ineffective at high frequencies.

III. THEORY

The Finite-Difference Time-Domain (FDTD) method is a robust and versatile numerical technique widely used to solve Maxwell's equations in the time domain. Introduced by K. S. Yee in 1966, the FDTD method discretizes both spatial and temporal domains using a grid, transforming continuous differential equations into a set of algebraic equations that can be solved iteratively. This method is particularly powerful for simulating complex electromagnetic phenomena in materials with varying properties over space and time.

In the FDTD method, the spatial domain is divided into a grid with cell dimensions Δx , Δy , and Δz , and the time domain is discretized with a time step Δt . The electric and magnetic fields are updated at each time step using finite-difference approximations of the derivatives. The updating equations for the electric and magnetic fields can be derived using central-difference approximations.

The stability of the FDTD method is governed by the Courant-Friedrichs-Lewy (CFL) condition, which ensures that the numerical solution remains stable. The general form of the CFL condition for a FDTD scheme in a homogeneous medium is given by:

$$\frac{c\Delta t}{\Delta \mathbf{r}} \leq 1. \quad (1a)$$

For a medium with a space-time varying refractive index, the stability criterion can be influenced by the variations in the refractive index. Therefore, the stability condition must take into account the maximum value of the refractive index over space and time to ensure stability throughout the simulation domain. The CFL condition can then be generalized to:

$$\frac{c\Delta t}{\Delta \mathbf{r} \cdot \max(n(\mathbf{I}; \mathbf{r}, t))} \leq 1, \quad (1b)$$

where $\max(n(\mathbf{I}; \mathbf{r}, t))$ represents the highest refractive index (slowest speed of light), and the CFL condition ensures that the time step Δt is small enough to accommodate this slowest propagation speed throughout the entire simulation domain. Equation (1b) yields

$$\Delta t \leq \frac{1}{c\sqrt{\frac{1}{\Delta x^2} + \frac{1}{\Delta y^2} + \frac{1}{\Delta z^2}} \cdot \max(n(\mathbf{I}; \mathbf{r}, t))}, \quad (1c)$$

where c is the speed of light in the medium. This condition implies that the time step Δt must be sufficiently small relative to the spatial discretization to ensure stability. The ratio $\max(\epsilon(\mathbf{I}; \mathbf{r}, t)/\mu(\mathbf{I}; \mathbf{r}, t))$ affects the wave propagation speed in the material, which must be considered to ensure stability.

The constitutive relations in the medium are:

$$\mathbf{D} = \epsilon_m(\mathbf{I}; \mathbf{r}, t)\mathbf{E} \quad (2a)$$

$$\mathbf{B} = \mu_m(\mathbf{I}; \mathbf{r}, t)\mathbf{H} \quad (2b)$$

$$\mathbf{J} = \sigma_m(\mathbf{I}; \mathbf{r}, t)\mathbf{E} \quad (2c)$$

Thus, the refractive index $n(\mathbf{I}; \mathbf{r}, t)$ of the medium is given by:

$$n(\mathbf{I}; \mathbf{r}, t) = c\sqrt{\mu_m(\mathbf{I}; \mathbf{r}, t) \left(\epsilon_m(\mathbf{I}; \mathbf{r}, t) - i\frac{\sigma_m(\mathbf{I}; \mathbf{r}, t)}{\omega} \right)} \quad (3)$$

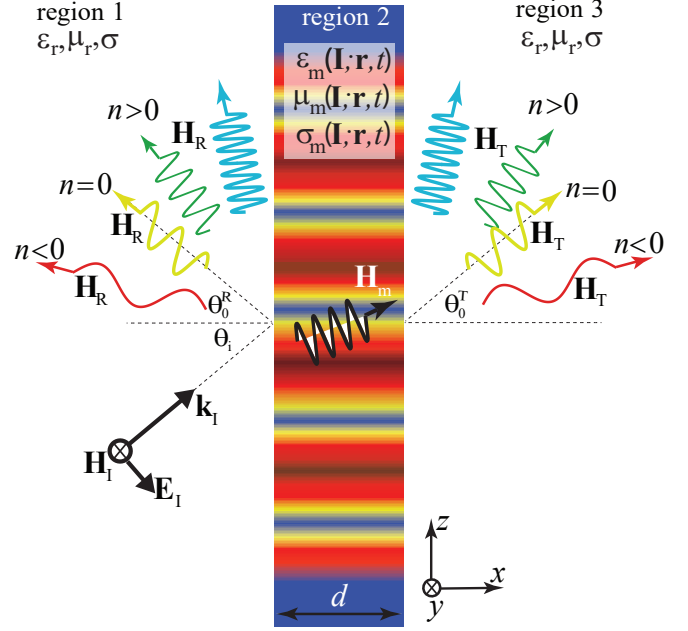


Fig. 2. Transverse magnetic (TM) electromagnetic wave incidence and scattering from a space-time-varying slab.

The fundamental Maxwell's equations in differential form for a medium are given by:

Faraday's law of induction:

$$\nabla \times \mathbf{E}_m = -\frac{\partial[\mu_m(\mathbf{I}; \mathbf{r}, t)\mathbf{H}_m]}{\partial t} \quad (4a)$$

and Ampère's law with Maxwell's addition:

$$\nabla \times \mathbf{H}_m = \frac{\partial[\epsilon_m(\mathbf{I}; \mathbf{r}, t)\mathbf{E}_m]}{\partial t} + \sigma_m(\mathbf{I}; \mathbf{r}, t)\mathbf{E}_m, \quad (4b)$$

where \mathbf{E}_m and \mathbf{H}_m are the electric and magnetic fields, respectively, while ϵ_m , μ_m , and σ_m are the time and space-dependent permittivity, permeability, and conductivity of the medium.

IV. FDTD SCHEME AND EQUATIONS FOR TM WAVE EXCITATION

Consider the generalized oblique incidence of a transverse magnetic (TM) electromagnetic wave on a space-time-varying slab, as depicted in Fig. 2, where

$$\mathbf{H} = \hat{\mathbf{y}}H_y(x, z, t), \quad (5a)$$

and

$$\mathbf{E} = -\eta \left[\hat{\mathbf{k}} \times \mathbf{H} \right] = \hat{\mathbf{x}}E_x(x, z, t) - \hat{\mathbf{z}}E_z(x, z, t). \quad (5b)$$

Therefore, Eqs. (4a) and (4b) yield

$$\mu(\mathbf{I}; \mathbf{r}, t) \frac{\partial H_y}{\partial t} + H_y \frac{\partial \mu(\mathbf{I}; \mathbf{r}, t)}{\partial t} = \frac{\partial E_z}{\partial x} - \frac{\partial E_x}{\partial z}, \quad (6a)$$

$$\epsilon(\mathbf{I}; \mathbf{r}, t) \frac{\partial E_x}{\partial t} + E_x \frac{\partial \epsilon(\mathbf{I}; \mathbf{r}, t)}{\partial t} = -\frac{\partial H_y}{\partial z} - \sigma(\mathbf{I}; \mathbf{r}, t)E_x, \quad (6b)$$

$$\epsilon(\mathbf{I}; \mathbf{r}, t) \frac{\partial E_z}{\partial t} + E_z \frac{\partial \epsilon(\mathbf{I}; \mathbf{r}, t)}{\partial t} = \frac{\partial H_y}{\partial x} - \sigma(\mathbf{I}; \mathbf{r}, t)E_z. \quad (6c)$$

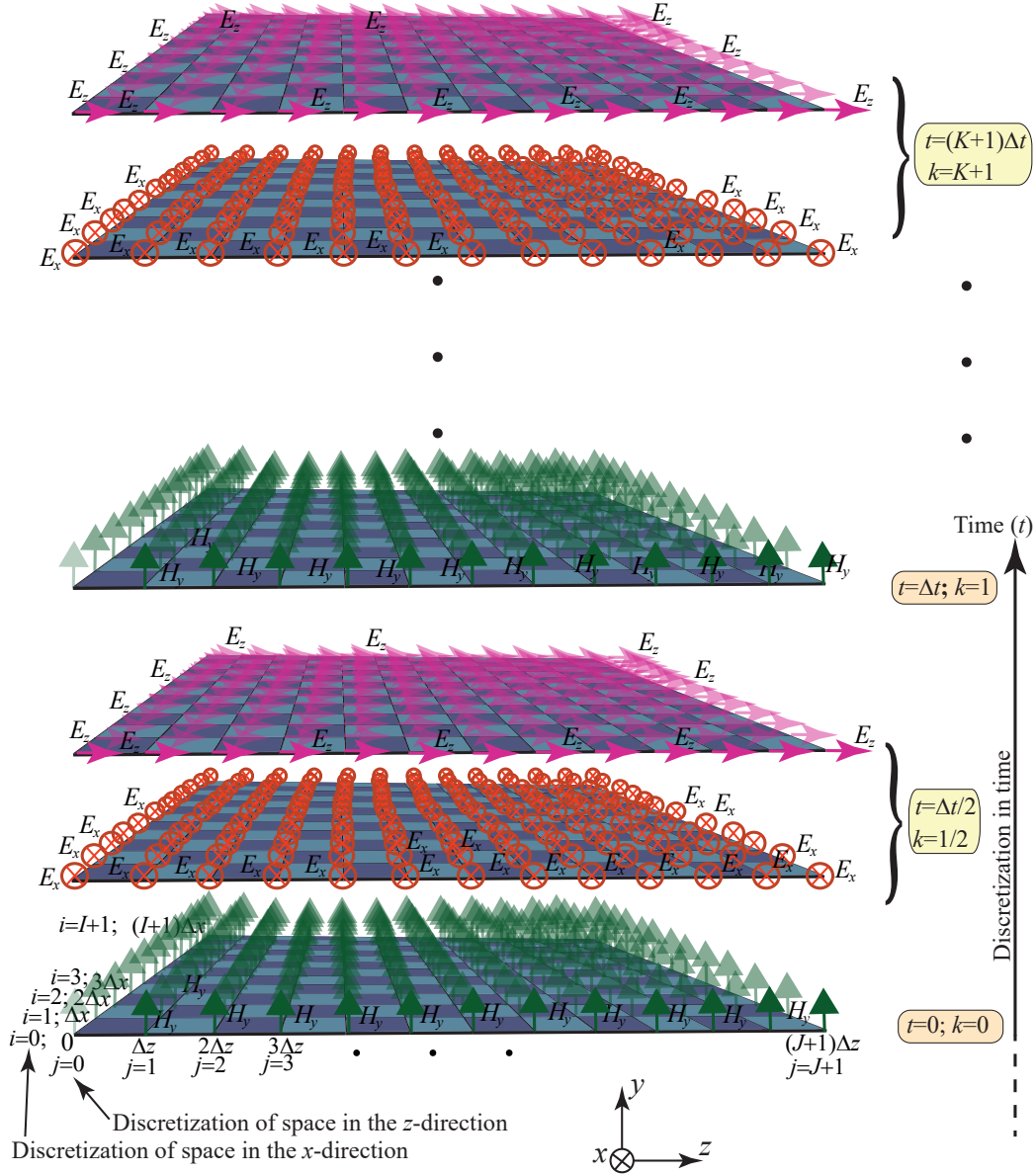


Fig. 3. Finite-difference time-domain scheme for TM wave illumination of a space-time-varying slab.

The finite-difference discretized form of the first two Maxwell's equations for the electric and magnetic fields will be simplified to

$$E_x \Big|_{i+1/2}^{k+1/2} = \left(1 - \Delta t \frac{\epsilon' + \sigma}{\epsilon} \Big|_{i+1/2}^k \right) E_x \Big|_{i+1/2}^{k-1/2} - \frac{\Delta t}{\epsilon \Big|_{i+1/2}^k} \frac{H_y \Big|_{i+1}^k - H_y \Big|_{i+1}^k}{\Delta z}, \quad (7a)$$

$$E_z \Big|_{i+1/2}^{k+1/2} = \left(1 - \Delta t \frac{\epsilon' + \sigma}{\epsilon} \Big|_{i+1/2}^k \right) E_z \Big|_{i+1/2}^{k-1/2} + \frac{\Delta t}{\epsilon \Big|_{i+1/2}^k} \frac{H_y \Big|_{i+1}^k - H_y \Big|_{i+1}^k}{\Delta x}, \quad (7b)$$

$$H_y \Big|_i^{k+1} = \left(1 - \Delta t \frac{\mu'}{\mu} \Big|_i^{k+1/2} \right) H_y \Big|_i^k - \frac{\Delta t}{\mu \Big|_i^{k+1/2}} \cdot \left(\frac{E_x \Big|_{i+1/2}^{k+1/2} - E_x \Big|_{i+1/2}^{k+1/2}}{\Delta z} - \frac{E_z \Big|_{i+1/2}^{k+1/2} - E_z \Big|_{i-1/2}^{k+1/2}}{\Delta x} \right). \quad (7c)$$

Figure 3 plots the implemented finite-difference time-domain scheme for numerical simulation of the oblique wave impinging to a general space-time-varying medium, where the electrical permittivity, magnetic permeability and electrical conductivity of the medium are all modulated in both space and time. We first discretize the medium to $J + 1$ spatial samples and $K + 1$ temporal samples, with the steps of Δz and Δt , respectively.

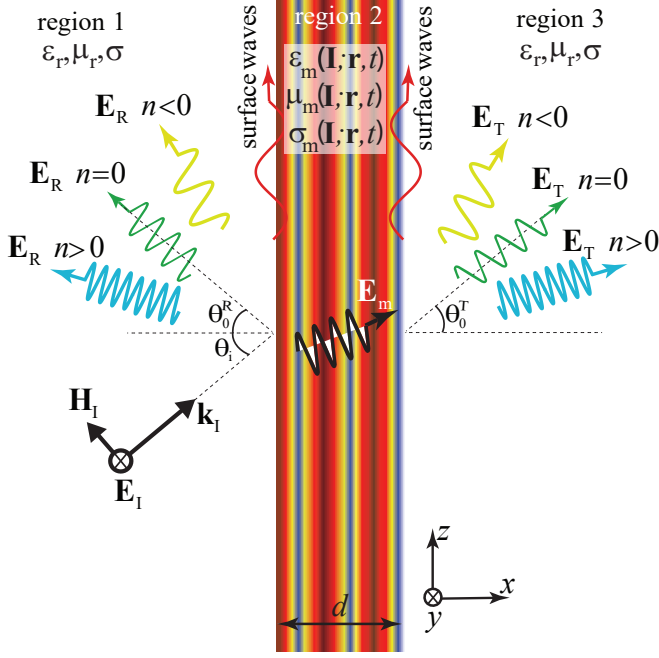


Fig. 4. Transverse electric (TE) wave incidence and scattering from a space-time-varying slab.

To analyze the signal's frequency components, we transform the output time-domain signal into its frequency-domain representation using the Fast Fourier Transform (FFT), as

$$E(\omega) = 20 \log_{10} |\mathcal{F}_{\text{shift}}(\mathcal{F}[E_{\text{out}}(t)])| \quad (8)$$

which provides the spectral content of the output signal E_{out} . The process begins with computing the Fast Fourier Transform (FFT) of E_{out} , transforming the signal from the time domain to the frequency domain. Following this, we apply a frequency shift using `fftshift`, centering the zero-frequency component in the spectrum, which facilitates better visualization and analysis. The magnitude of the resulting complex frequency components is then calculated, converting them into real-valued amplitudes. To represent the data in a more perceptually meaningful way, we convert the scaled magnitudes into a logarithmic scale using the base-10 logarithm. Finally, the factor of 20 is applied to express these values in decibels (dB), providing a logarithmic measure of the signal's frequency content. This approach allows for a comprehensive and intuitive understanding of the signal's behavior in the frequency domain, highlighting the relative strengths of various frequency components in a manner that aligns with human auditory perception.

V. FDTD SCHEME AND EQUATIONS FOR TE WAVE EXCITATION

Next, Consider the generalized oblique incidence of a transverse electric (TE) electromagnetic wave on a space-time-varying slab, as depicted in Fig. 4. The electric and magnetic fields read

$$\mathbf{E} = \hat{\mathbf{y}}E_y(x, z, t), \quad (9a)$$

and

$$\mathbf{H} = \frac{1}{\eta} [\hat{\mathbf{k}} \times \mathbf{E}] = -\hat{x}H_x(x, z, t) + \hat{z}H_z(x, z, t). \quad (9b)$$

Consequently, Eqs. (4a) and (4b) yield

$$\epsilon(\mathbf{I}; \mathbf{r}, t) \frac{\partial E_y}{\partial t} + E_y \frac{\partial \epsilon(\mathbf{I}; \mathbf{r}, t)}{\partial t} = \frac{\partial H_x}{\partial z} - \frac{\partial H_z}{\partial x} - \sigma(\mathbf{I}; \mathbf{r}, t) E_y, \quad (10a)$$

$$\mu(\mathbf{I}; \mathbf{r}, t) \frac{\partial H_x}{\partial t} + H_x \frac{\partial \mu(\mathbf{I}; \mathbf{r}, t)}{\partial t} = \frac{\partial E_y}{\partial z}, \quad (10b)$$

$$\mu(\mathbf{I}; \mathbf{r}, t) \frac{\partial H_z}{\partial t} + H_z \frac{\partial \mu(\mathbf{I}; \mathbf{r}, t)}{\partial t} = -\frac{\partial E_y}{\partial x}. \quad (10c)$$

Figure 5 plots the implemented finite-difference time-domain scheme for numerical simulation of the general oblique TE wave impinging to a general space-time-varying medium, where the electrical permittivity, magnetic permeability and electrical conductivity of the medium are all modulated in both space and time. The finite-difference discretized form of the first two Maxwell's equations for the electric and magnetic fields read

$$H_x \Big|_{i+1/2}^{k+1/2} = \left(1 - \Delta t \frac{\mu'}{\mu} \Big|_{i+1/2}^k \right) H_x \Big|_{i+1/2}^{k-1/2} + \frac{\Delta t}{\mu \Big|_{i+1/2}^k} \frac{E_y \Big|_{i+1}^k - E_y \Big|_i^k}{\Delta z}, \quad (11a)$$

$$H_z \Big|_{i+1/2}^{k+1/2} = \left(1 - \Delta t \frac{\mu'}{\mu} \Big|_{i+1/2}^k \right) H_z \Big|_{i+1/2}^{k-1/2} - \frac{\Delta t}{\mu \Big|_{i+1/2}^k} \frac{E_y \Big|_{i+1}^k - E_y \Big|_i^k}{\Delta x}, \quad (11b)$$

$$E_y \Big|_i^{k+1} = \left(1 - \Delta t \frac{\epsilon' + \sigma}{\epsilon} \Big|_i^{k+1/2} \right) E_y \Big|_i^k + \frac{\Delta t}{\epsilon \Big|_i^{k+1/2}} \cdot \left(\frac{H_x \Big|_{i+1/2}^{k+1/2} - H_x \Big|_{i+1/2}^{k-1/2}}{\Delta z} - \frac{H_z \Big|_{i+1/2}^{k+1/2} - H_z \Big|_{i-1/2}^{k+1/2}}{\Delta x} \right). \quad (11c)$$

VI. ILLUSTRATIVE EXAMPLES

A. Multifunctional Operation

As an illustrative example, we investigate the effect of wave illumination on a nonlinear space-time-varying permittivity described by the equation:

$$\epsilon_m(z, t) = \epsilon_0 \epsilon_r (1 + \delta_\epsilon \cos[\beta_m z - \omega_m t + \phi]), \quad (12)$$

where μ and σ of the slab remain invariant with respect to space and time. In Fig. 6, we depict the generalized oblique wave incidence and transmission from the slab, with the permittivity described by Equation (12), where $\omega_m > \omega_0$, leading to the intriguing functionality resembling an antenna-mixer-amplifier. This setup facilitates the transition of space-time harmonics from a propagating wave to a space-time surface wave at a lower frequency within the modulated medium.

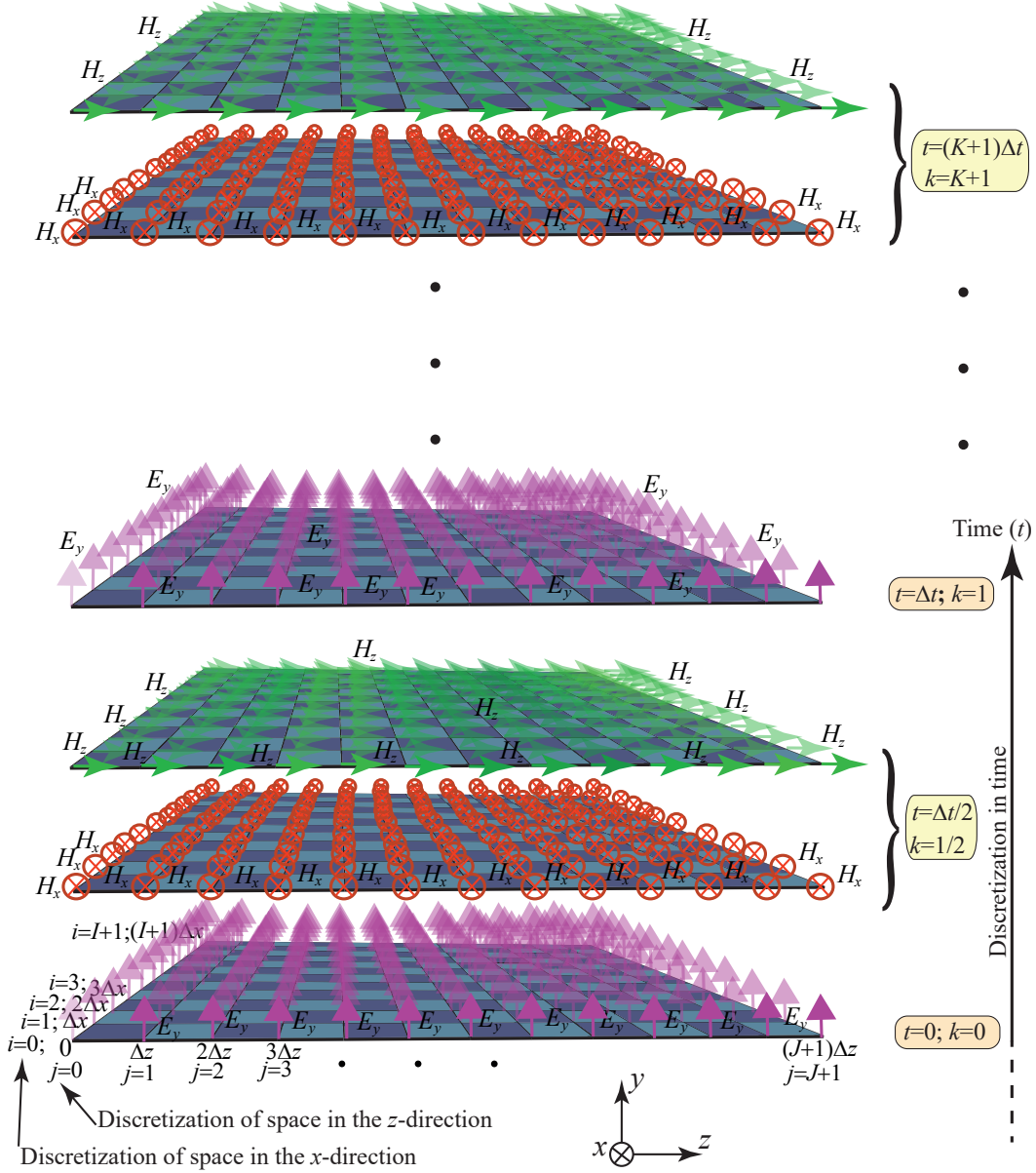


Fig. 5. Finite-difference time-domain scheme for oblique incidence of TE wave to a space-time-modulated slab.

B. Unidirectional Generation of Space-Time Harmonics

To demonstrate nonreciprocal and asymmetric wave transmission of space-time-varying slabs, we investigate the effect of TE wave illumination on a linear permittivity-and-permeability space-time-varying described space-time-varying permittivity in (12) and space-time-varying permeability:

$$\mu_m(z, t) = \mu_0 \mu_r (1 + \delta_\mu \cos[\beta_m z - \omega_m t + \phi]), \quad (13)$$

with the conductivity (σ) of the slab remaining invariant with respect to space and time. Figures 7(a) and 7(b) present the result of 1D-space FDTD investigation into the nonreciprocal wave transmission characteristics from the slab. Here, $\omega_m \ll \omega_0$, leading to generation of space-time harmonics in the forward case (Fig.7(a)), while no such generation occurs in the backward case (Fig.7(b)).

C. Nonreciprocal Beam-splitter

Figures 8(a) and 8(b) showcase another application of space-time-varying slabs: unidirectional beamsplitting for $\omega_m > \omega_0$, with the permittivity defined by Eq. (12), where $\omega_m = 2\omega_0$. Here, the incident wave from the bottom is transmitted while undergoing beam splitting. Consequently, the transmitted beam retains the same frequency as the incident wave, namely ω_0 .

D. Space-Time-Modulated Diffraction Grating

Fig. 9(a) shows FDTD time-domain and frequency spectrum results for wave diffraction from a space-time-periodic grating with traveling space-time permittivity modulation, where the modulation travels along the $+x$ direction, from left to right. The 2D time-domain results in Fig. 9(a) clearly demonstrate that spatial diffractions are directed to the right side of the

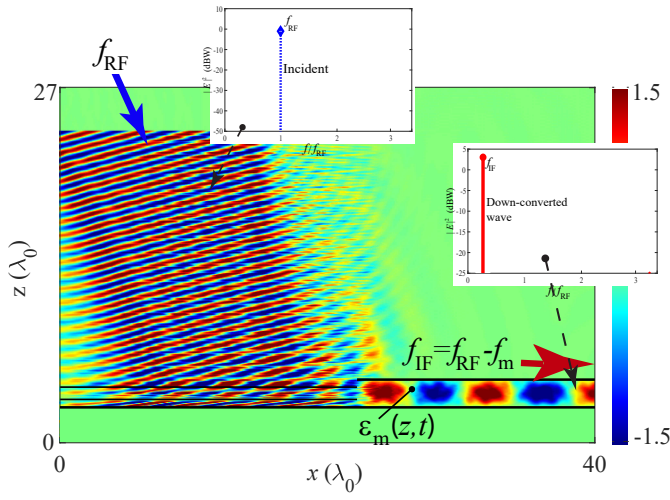
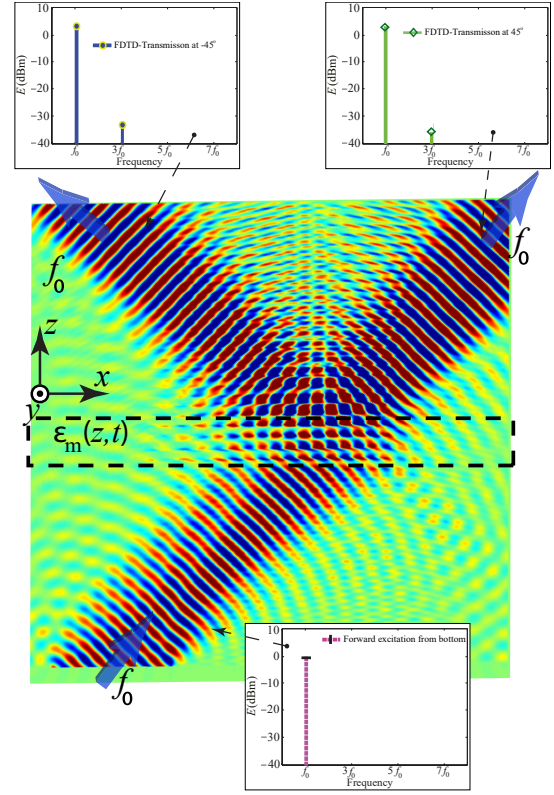
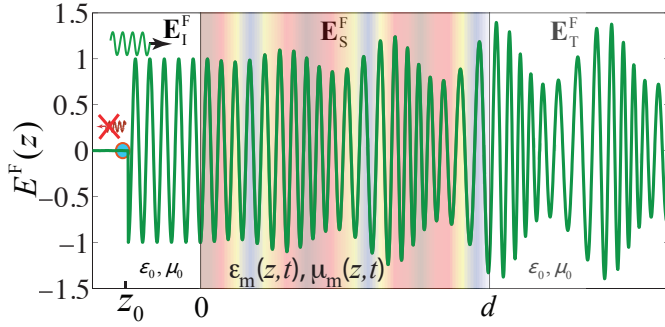


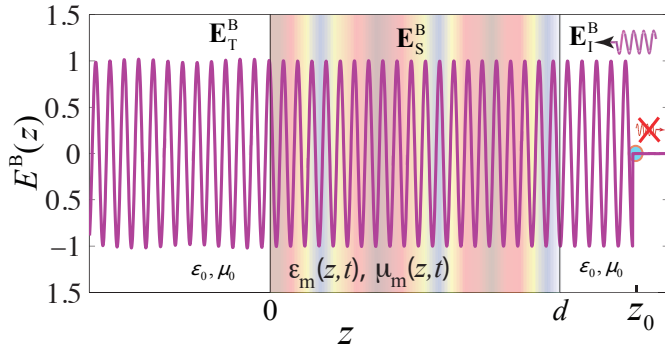
Fig. 6. FDTD time-domain 2D results and frequency spectrum for antenna-mixer-amplifier functionality of space-time-modulated permittivity slab.



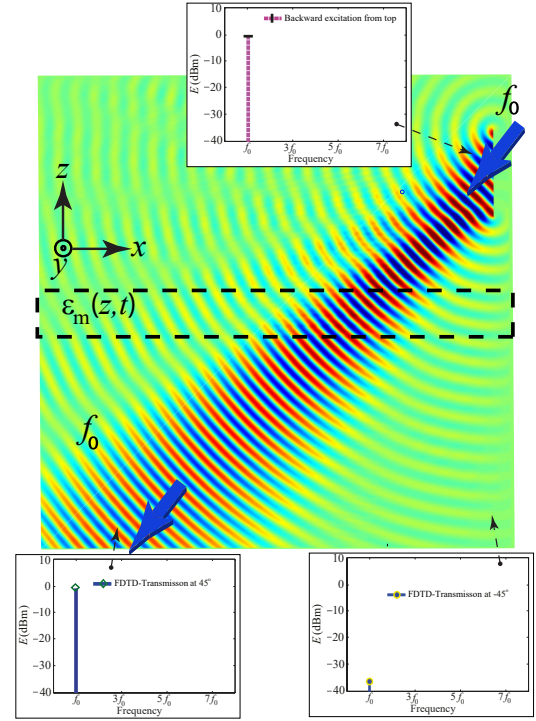
(a)



(a)



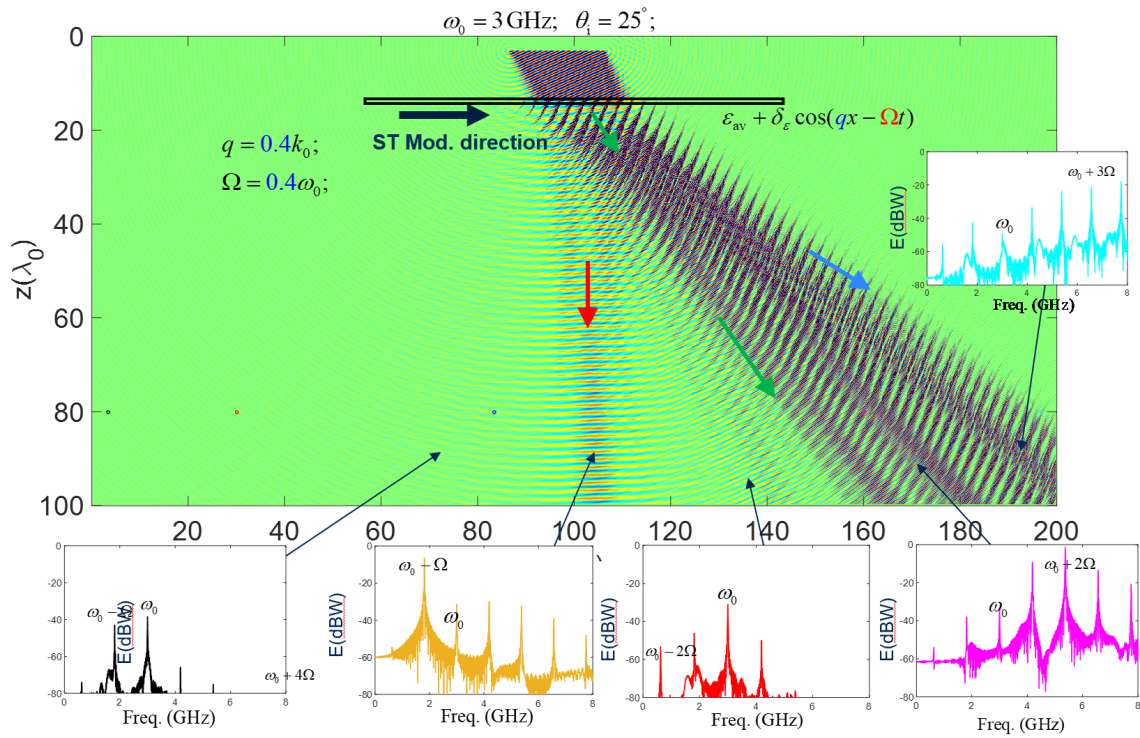
(b)



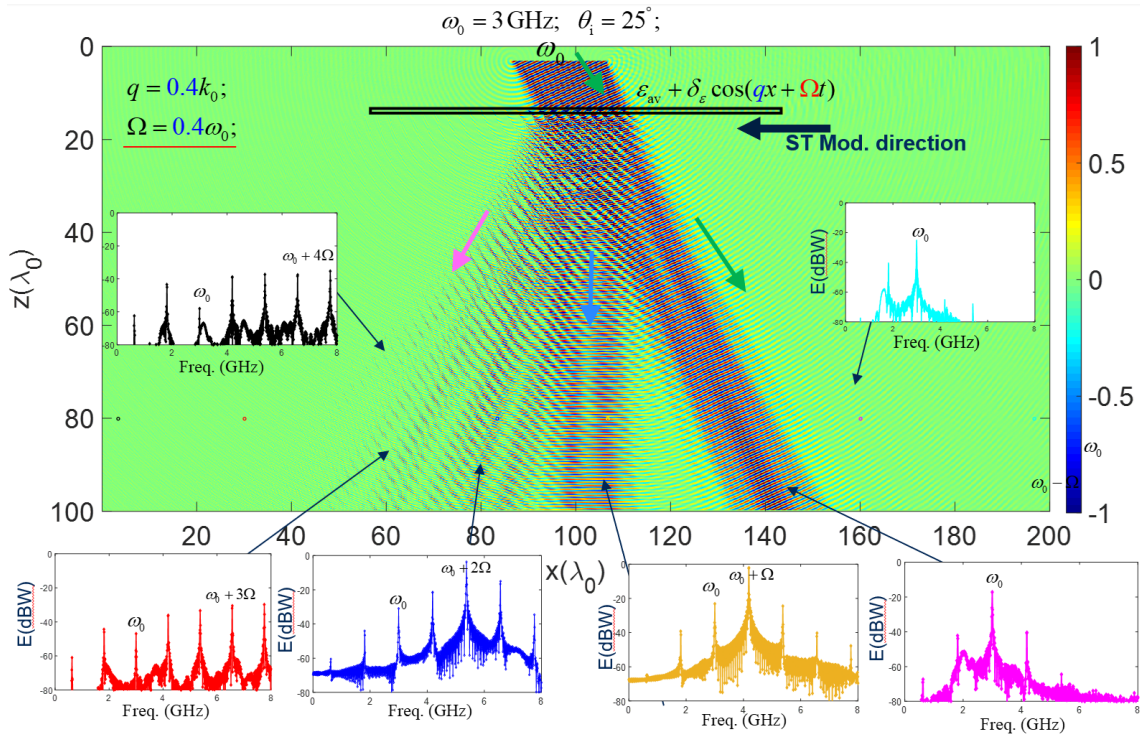
(b)

Fig. 7. FDTD time-domain 1D results for normal incidence demonstrating nonreciprocal wave transmission from a space-time-modulated slab. (a) Forward wave transmission. (b) Backward wave transmission.

Fig. 8. FDTD time-domain 2D results and frequency spectrum for beam splitting functionality of a space-time-modulated permittivity slab. (a) Forward excitation from the bottom-left. (b) Backward excitation from the top-right.



(a)



(b)

Fig. 9. FDTD time-domain 2D results and frequency spectrum for nonreciprocal spatiotemporal diffraction from a space-time-periodic permittivity-modulated diffraction grating: (a) The modulation travels along the $+x$ direction, from left to right. (b) The modulation travels along the $-x$ direction, from right to left.

grating. This indicates that the traveling modulation in the $+x$ direction imparts momentum to the diffracted waves, causing them to propagate in the same direction. The frequency spectrum results, shown as insets in Fig. 9(a), reveal that these spatial diffractions include an infinite number of $\omega_0 \pm n\Omega$ time diffractions ($-\infty < n < +\infty$). Among these, one temporal diffraction is particularly strong and dominant. This dominance suggests that the energy of the incident wave is primarily transferred into this specific temporal harmonic, resulting in a pronounced diffraction peak.

Fig. 9(b) presents FDTD time-domain and frequency spectrum results for wave diffraction from a space-time-periodic grating with traveling space-time permittivity modulation, where the modulation travels along the $-x$ direction, from left to right. The 2D time-domain results in Fig. 9(b) show that spatial diffractions are directed toward the left side of the main incident wave propagating at an angle of 30° . This behavior indicates that the traveling modulation in the $-x$ direction induces a momentum transfer in the opposite direction of the modulation travel, causing the diffracted waves to propagate leftward. The frequency spectrum results, shown as insets in Fig. 9(b), indicate that these spatial diffractions also include an infinite number of $\omega_0 \pm n\Omega$ time diffractions. Similar to the previous case, one temporal diffraction is notably stronger and dominant. This suggests a consistent mechanism where the traveling modulation selectively enhances a particular temporal harmonic, concentrating the energy into this dominant diffraction mode.

The FDTD simulations provide clear insights into the behavior of asymmetric and nonreciprocal wave diffraction from space-time-periodic gratings with traveling permittivity modulations. When the modulation travels in the $+x$ direction, spatial diffractions are directed to the right, aligning with the modulation direction. Conversely, when the modulation travels in the $-x$ direction, the spatial diffractions are directed leftward, opposite to the modulation direction. In both cases, the frequency spectrum analysis reveals the presence of an infinite number of $\omega_0 \pm n\Omega$ time diffractions. However, one temporal diffraction consistently emerges as stronger and dominant. This dominance can be attributed to the resonant interaction between the incident wave and the traveling modulation, which selectively amplifies a specific temporal harmonic. These results highlight the critical role of modulation direction in controlling the spatial and temporal characteristics of diffracted waves. Such control mechanisms could be exploited in the design of advanced wave manipulation devices, including beam steerers, frequency converters, and modulators, for applications in communication systems and photonic circuits.

VII. CONCLUSION

We have provided a comprehensive investigation into the Finite Difference Time Domain (FDTD) numerical modeling of electromagnetic wave transmission through linear and nonlinear space-time-varying gratings. Through the provided FDTD scheme and electromagnetic fields update equations for both TM and TE wave illuminations, we enable re-

searchers and engineers to simulate and analyze the behavior of space-time-varying slabs with ease. Moreover, the illustrative examples presented in this paper highlight the diverse functionality and applications of these components, which could be further extended to incorporate advanced materials like superconductors and perovskites for potential use in optoelectronic and quantum technologies [52], [53]. We believe that the insights provided in this paper will inspire further research and development in the field of space-time-varying microwave components, paving the way for innovative solutions in next-generation wireless communication systems, biomedicine, radars, and quantum technologies.

REFERENCES

- [1] S. Taravati and A. A. Kishk, "Space-time modulation: Principles and applications," *IEEE Microw. Mag.*, vol. 21, no. 4, pp. 30–56, 2020.
- [2] J. Wang, D. Feng, Y. Kong, S. Quan, and S. Xing, "Imaging properties of nonperiodic time-varying active frequency selective surface," *IEEE Transactions on Antennas and Propagation*, vol. 70, no. 7, pp. 5884–5891, 2022.
- [3] S. Taravati, "Giant linear nonreciprocity, zero reflection, and zero band gap in equilibrated space-time-varying media," *Phys. Rev. Appl.*, vol. 9, no. 6, p. 064012, Jun. 2018.
- [4] M. Saikia and K. V. Srivastava, "A time-modulated polarization-rotating frequency-selective surface," *IEEE Transactions on Antennas and Propagation*, vol. 71, no. 2, pp. 1506–1515, 2022.
- [5] S. Taravati and A. A. Kishk, "Dynamic modulation yields one-way beam splitting," *Phys. Rev. B*, vol. 99, no. 7, p. 075101, Jan. 2019.
- [6] S. Taravati and G. V. Eleftheriades, "Generalized space-time periodic diffraction gratings: Theory and applications," *Phys. Rev. Appl.*, vol. 12, no. 2, p. 024026, 2019.
- [7] S. Taravati and A. A. Kishk, "Advanced wave engineering via obliquely illuminated space-time-modulated slab," *IEEE Trans. Antennas Propag.*, vol. 67, no. 1, pp. 270–281, 2019.
- [8] S. Taravati and G. V. Eleftheriades, "Space-time medium functions as a perfect antenna-mixer-amplifier transceiver," *Phys. Rev. Appl.*, vol. 14, no. 5, p. 054017, 2020.
- [9] R. Sabri, M. M. Salary, and H. Mosallaei, "Broadband continuous beam-steering with time-modulated metasurfaces in the near-infrared spectral regime," *APL Photonics*, vol. 6, no. 8, p. 086109, 2021.
- [10] S. Taravati and G. V. Eleftheriades, "Full-duplex nonreciprocal beam steering by time-modulated phase-gradient metasurfaces," *Phys. Rev. Appl.*, vol. 14, no. 1, p. 014027, 2020.
- [11] X. Wang, V. S. Asadchy, S. Fan, and S. A. Tretyakov, "Space-time metasurfaces for power combining of waves," *ACS Photonics*, vol. 8, no. 10, pp. 3034–3041, 2021.
- [12] S. Taravati and G. V. Eleftheriades, "Programmable nonreciprocal metaprism," *Sci. Rep.*, vol. 11, no. 1, pp. 1–12, 2021.
- [13] S. Wan, L. Cao, Y. Zhu, M. Oudich, and B. Assouar, "Nonreciprocal sound propagation via cascaded time-modulated slab resonators," *Phys. Rev. Appl.*, vol. 16, no. 6, p. 064061, 2021.
- [14] S. Taravati, "Self-biased broadband magnet-free linear isolator based on one-way space-time coherency," *Phys. Rev. B*, vol. 96, no. 23, p. 235150, Dec. 2017.
- [15] S. Taravati and G. V. Eleftheriades, "4D wave transformations enabled by space-time metasurfaces: Foundations and illustrative examples," *IEEE Antennas and Propagation Magazine*, vol. 65, no. 4, pp. 61–74, 2023.
- [16] C. Amra, A. Passian, P. Tchamitchian, M. Ettore, A. Alwakil, J. A. Zapien, P. Rouquette, Y. Abautret, and M. Zerrad, "Linear-frequency conversion with time-varying metasurfaces," *Physical Review Research*, vol. 6, no. 1, p. 013002, 2024.
- [17] S. Taravati and G. V. Eleftheriades, "Full-duplex reflective beamsteering metasurface featuring magnetless nonreciprocal amplification," *Nat. Commun.*, vol. 14, p. 4414, 2021.
- [18] S. Taravati and G. V. Eleftheriades, "Reflective beam-steering metasurface," Feb. 29 2024, US Patent App. 18/260,958.
- [19] M. Valizadeh, L. Yousefi, and M. Miri, "Analytical formulation of spatiotemporal modulated graphene-based waveguides using floquet-bloch theory," *Scientific Reports*, vol. 14, no. 1, p. 7332, 2024.

- [20] H. A. Lorentz, "Electromagnetic phenomena in a system moving with any velocity smaller than that of light," in *Collected Papers*. Springer, 1937, pp. 172–197.
- [21] C. Elachi, "Electromagnetic wave propagation and wave-vector diagram in space-time periodic media," *IEEE Trans. Antennas Propagat.*, vol. 20, no. 4, pp. 534–536, 1972.
- [22] —, "Waves in active and passive periodic structures: A review," *Proc. IEEE*, vol. 64, no. 12, pp. 1666–1698, 1976.
- [23] S. Taravati, N. Chamanara, and C. Caloz, "Nonreciprocal electromagnetic scattering from a periodically space-time modulated slab and application to a quasisonic isolator," *Phys. Rev. B*, vol. 96, no. 16, p. 165144, Oct. 2017.
- [24] A. Darvish and A. Kishk, "Modern shielding methods: On applications of space-time modulated media," *IEEE Transactions on Antennas and Propagation*, 2024.
- [25] M. Oudich, N. J. Gerard, Y. Deng, and Y. Jing, "Tailoring structure-borne sound through bandgap engineering in phononic crystals and metamaterials: a comprehensive review," *Advanced Functional Materials*, vol. 33, no. 2, p. 2206309, 2023.
- [26] P. A. Huidobro, E. Galiffi, S. Guenneau, R. V. Craster, and J. Pendry, "Fresnel drag in space-time-modulated metamaterials," *Proc. Natl. Acad. Sci. U.S.A.*, vol. 116, no. 50, pp. 24 943–24 948, 2019.
- [27] S. A. Stewart, T. J. Smy, and S. Gupta, "Finite-difference time-domain modeling of space-time-modulated metasurfaces," *IEEE Trans. Antennas Propagat.*, vol. 66, no. 1, pp. 281–292, 2017.
- [28] D. M. Solís and N. Engheta, "Functional analysis of the polarization response in linear time-varying media: A generalization of the kramers-kronig relations," *Physical Review B*, vol. 103, no. 14, p. 144303, 2021.
- [29] V. Pacheco-Peña and N. Engheta, "Temporal equivalent of the brewster angle," *Physical Review B*, vol. 104, no. 21, p. 214308, 2021.
- [30] M. Saikia, K. V. Srivastava, and S. A. Ramakrishna, "Frequency-shifted reflection of electromagnetic waves using a time-modulated active tunable frequency-selective surface," *IEEE Trans. Antennas Propagat.*, vol. 68, no. 4, pp. 2937–2944, 2019.
- [31] A. E. Cardin, S. R. Silva, S. R. Vardeny, W. J. Padilla, A. Saxena, A. J. Taylor, W. J. Kort-Kamp, H.-T. Chen, D. A. Dalvit, and A. K. Azad, "Surface-wave-assisted nonreciprocity in spatio-temporally modulated metasurfaces," *Nature communications*, vol. 11, no. 1, p. 1469, 2020.
- [32] S. Taravati and G. V. Eleftheriades, "Microwave space-time-modulated metasurfaces," *ACS Photonics*, vol. 9, no. 2, pp. 305–318, 2022.
- [33] A. Kumar, S. Kongari, Y. Chandrapure, and D. Sarkar, "Multi-functional metasurface as a transmissive/reflective fss and an on-air frequency mixer," *Scientific Reports*, vol. 14, no. 1, p. 13874, 2024.
- [34] M. M. Salary and H. Mosallaei, "Time-modulated conducting oxide metasurfaces for adaptive multiple access optical communication," *IEEE Trans. Antennas Propagat.*, vol. 68, no. 3, pp. 1628–1642, 2020.
- [35] J. Sisler, P. Thureja, M. Y. Grajower, R. Sokhoyan, I. Huang, and H. A. Atwater, "Electrically tunable space-time metasurfaces at optical frequencies," *Nature Nanotechnology*, pp. 1–8, 2024.
- [36] S. Taravati and G. V. Eleftheriades, "Nonreciprocal beam steerable metasurfaces," Dec. 21 2023, US Patent App. 18/035,826.
- [37] X. Wang, M. S. Tong, and L. Zhao, "Pseudorandom noise sequence time-modulated reflective metasurfaces for target recognition," *IEEE Transactions on Microwave Theory and Techniques*, vol. 71, no. 8, pp. 3446–3454, 2023.
- [38] S. Taravati and G. V. Eleftheriades, "Lightweight low-noise linear isolator integrating phase-and amplitude-engineered temporal loops," *Adv. Mater. Technol.*, p. 2100674, 2021.
- [39] V. Pacheco-Peña and N. Engheta, "Temporal aiming," *Light: Science & Applications*, vol. 9, no. 1, p. 129, 2020.
- [40] S. Taravati and G. V. Eleftheriades, "Pure and linear frequency-conversion temporal metasurface," *Phys. Rev. Appl.*, vol. 15, no. 6, p. 064011, 2021.
- [41] S. Taravati, "Aperiodic space-time modulation for pure frequency mixing," *Phys. Rev. B*, vol. 97, no. 11, p. 115131, 2018.
- [42] M. J. Mencagli, D. L. Sounas, M. Fink, and N. Engheta, "Static-to-dynamic field conversion with time-varying media," *Physical Review B*, vol. 105, no. 14, p. 144301, 2022.
- [43] T. Dinc, A. Nagulu, and H. Krishnaswamy, "A millimeter-wave non-magnetic passive soi cmos circulator based on spatio-temporal conductivity modulation," *IEEE J. Solid-State Circuits*, vol. 52, no. 12, pp. 3276–3292, 2017.
- [44] S. Taravati and G. V. Eleftheriades, "Low-noise and linear nonmagnetic circulator by a temporal nonreciprocal phase shifter," *Physical Review Applied*, vol. 18, no. 3, p. 034082, 2022.
- [45] X. Zhu, J. Li, C. Shen, G. Zhang, S. A. Cummer, and L. Li, "Tunable unidirectional compact acoustic amplifier via space-time modulated membranes," *Phys. Rev. B*, vol. 102, no. 2, p. 024309, 2020.
- [46] J. Pendry, E. Galiffi, and P. Huidobro, "A new mechanism for gain in time dependent media," *arXiv preprint arXiv:2009.12077*, 2020.
- [47] H. B. Sedeh, M. M. Salary, and H. Mosallaei, "Active multiple access secure communication enabled by graphene-based time-modulated metasurfaces," *IEEE Trans. Antennas Propagat.*, vol. 70, no. 1, pp. 664–679, 2021.
- [48] J. Zang, A. Alvarez-Melcon, and J. Gómez-Díaz, "Nonreciprocal phased-array antennas," *Phys. Rev. Appl.*, vol. 12, no. 5, p. 054008, 2019.
- [49] J. Zang, X. Wang, A. Alvarez-Melcon, and J. S. Gómez-Díaz, "Nonreciprocal yagi-uda filtering antennas," *IEEE Antennas Wirel. Propagat. Lett.*, vol. 18, no. 12, pp. 2661–2665, 2019.
- [50] L. Zhang, Z. X. Wang, R. W. Shao, J. L. Shen, X. Q. Chen, X. Wan, Q. Cheng, and T. J. Cui, "Dynamically realizing arbitrary multi-bit programmable phases using a 2-bit time-domain coding metasurface," *IEEE Trans. Antennas Propagat.*, vol. 68, no. 4, pp. 2984–2992, 2019.
- [51] S. Taravati and C. Caloz, "Mixer-duplexer-antenna leaky-wave system based on periodic space-time modulation," *IEEE Trans. Antennas Propagat.*, vol. 65, no. 2, pp. 442 – 452, Feb. 2017.
- [52] J. Clarke and F. K. Wilhelm, "Superconducting quantum bits," *Nature*, vol. 453, no. 7198, pp. 1031–1042, 2008.
- [53] K. Fallah, S. Norouziyan Alam, B. Ghaffary, F. Yekekar, S. Taghiyan, and S. Taravati, "Enhancement of the environmental stability of perovskite thin films via az5214-photoresist and pmma coatings," *Opt. Mater. Express*, vol. 14, no. 8, pp. 2083–2094, 2024.